Gravity wave influence on the global structure of the diurnal tide in the mesosphere and lower thermosphere

DAVID A ORTLAND

Northwest Research Associates

14508 NE 20th St

Bellevue, Washington 98006

ortland@nwra.com

and

M. JOAN ALEXANDER

Colorado Research Associates

3380 Mitchell Lane

Boulder, Colorado 80301

alexand@cora.nwra.com

Abstract

Observations of the diurnal tide from instruments aboard the Thermosphere, Ionosphere, Mesosphere, Energetics and Dynamics (TIMED) explorer and from the Upper Atmosphere Research Satellite (UARS) show that the vertical wavelength of the tide is significantly shorter than what is predicted by tidal theory. The observed vertical structure of the tide can be reproduced in a mechanistic model by including gravity wave interaction. The model tide amplitude and phase are sensitive to the amplitude and phase of the diurnal component of momentum forcing that arises from gravity wave breaking. The phase of the momentum forcing relative to the tide determines whether the tide amplitude is increased or diminished by gravity wave forcing, while the amplitude of the momentum forcing determines how rapidly the tide phase will change with height. The momentum forcing profile is shaped by the structure of the gravity wave source spectrum. By comparing both the model tide amplitude and phase profiles to observations, we can provide constraints on both the gravity wave source spectrum that should be used in a gravity wave parameterization scheme and on the eddy diffusion that acts on the tide. We examine differences between the effects that two gravity wave schemes have on the tide. The role that gravity waves may play in producing tide variability is discussed in light of the results presented here.

1. Introduction

It has long been known that the diurnal tide modulates gravity wave (GW) fluxes in the mesosphere (Fritts and Vincent, 1987; Wang and Fritts, 1991; Isler and Fritts, 1999), but there is still some debate as to how much this flux modulation affects the tide itself. It is fairly well accepted that GW breaking influences tide structure by effectively creating mean background eddy diffusion, even though the strength and vertical profile of this diffusion is not yet agreed upon (e.g. McLandress 2002a; Akmaev 2001). Localized GW effects on the tide may also arise from tidal modulation of the wave breaking and heat fluxes, causing temperature inversions (Liu and Hagan, 1998). The tidal modulation of the GW momentum fluxes will produce a gravity wave induced momentum forcing of the tide that is still not well understood, and will be the focus of this paper.

Several mechanistic and general circulation model (GCM) studies have been performed that examine the effect of gravity waves on the diurnal tide. These studies have used a variety of GW parameterizations in order to simulate the gravity wave forcing, since the gravity waves act on a scale much smaller than the grid size of the models. Unfortunately, conflicting conclusions arise from these studies because of differences in the GW source setting or because of inherent differences between the underlying assumptions on which the schemes are based. For example, McLandress (1998) noted that mechanistic model experiments employing the Lindzen GW parameterization reduced tidal amplitude while those employing the Hines parameterization enhance tidal amplitude. This inability to accurately quantify both the momentum and diffusive forcing of gravity waves has added to the debate on whether or not gravity waves are responsible for the observed seasonal variability of the diurnal tide (McLandress 2002a,b and refs.) In all of these studies, the GW parameterization was tuned to produce a realistic model mean flow, and then it was assumed that this tuning would produce a realistic simulation of the interaction between the model GW and tide.

Recently there have been many studies that examine how to bring a mechanistic tide model to agree with the observations made by instruments aboard the Upper Atmosphere Research Satellite (UARS) (e.g. Khattatov et al., 1997; Yudin et al., 1997, Akmaev et al., 1997; Hagan et al., 1999). In all of these studies, the vertical amplitude

profile of the model tide is made to align with the observed amplitude by adjusting dissipation parameters, but the tidal phase in the model was not examined in detail. However, in our recent attempts to match tidal model simulations to observations of the global tidal wind and temperature fields as seen by UARS and the Thermosphere Ionosphere Mesosphere Energetics and Dynamics (TIMED) instruments, we have found that a close examination of the model phase is crucial for quantifying the effect of GW interaction with the tide. These observations show quite clearly that the vertical wavelength of the tide is much shorter than can realistically be simulated in a model that does not account for GW momentum forcing of the tide. The discrepancy between a tide model (to be described below) and observations from UARS and TIMED is illustrated in Figure 1. The top two panels of this figure show UARS High Resolution Doppler Imager (HRDI) meridional winds on the left and TIMED Doppler Imager (TIDI) meridional winds on the right. The winds were binned at 9 hours local time for the month of March (1993 for HRDI and 2004 for TIDI). The bottom two panels show model simulations with and without GW forcing for comparison.

Many modelers have noted that GW momentum forcing advances the phase of the tide. As the phase advance increases in a region where the GW force is strong we see a shortening of the local vertical wavelength of the tide. One explanation for why GW forcing affects the tide wavelength is provided by Ortland (2005a,b). No other known influences on the tide can account for a shortened wavelength. Tide forcing due to GW diffusion affects the tide amplitude profile and typically acts to increase tide wavelength. The wavelength can also be modulated somewhat by the background zonal mean temperature structure, since it is inversely proportional to the buoyancy frequency. However, the buoyancy frequency decreases in the mesosphere and therefore also acts to increase tide wavelength.

We must conclude that GW momentum forcing plays an important role in shaping global tide structure. In order to accurately include GW effects in a tidal model, it is clear that the GW parameterizations must be further tuned to ensure that they not only produce the observed mean wind and temperature structure, which constrains the source structure of GWs propagating in the zonal direction, but that they also produce the observed effects on tidal structure. The tidal observations thus place important new

constraints on the GW source spectra that are used in a GW parameterization scheme. The purpose of this paper is to provide a systematic examination of how the GW momentum forcing profile depends on the source spectrum and then how this forcing profile shapes the vertical structure of the diurnal tide.

There are details in the observed tidal structure that provide insight into the magnitude of the GW interaction with the tide. First, the wavelength shortening is observed to occur in a restricted altitude range between 70 and 100 km. This implies that significant GW breaking must occur in this altitude range, and some inferences can then be made regarding the magnitude of the GW momentum force that is responsible. Second, it was shown by Ortland (2005b) that globally uniform GW forcing should cause the horizontal scale of the tide to decrease. The horizontal scale of the tide seen by TIMED is shorter than it is for the classical Hough modes, giving another indication that GWs affect the tide. Finally, the phase structure of the diurnal tide is directly related to the amplitude of the diurnal component of the GW momentum force. The amplitude profile of the diurnal tide is related to the dissipation mechanisms that act on the tide. It will be shown that whether the GW momentum force amplifies or diminishes tide amplitude will depend on the relative phase between the tide and the diurnal component of the GW force. The phase relationship between tide and GW force will depend on the GW source structure as well as the GW saturation mechanism built into a particular parameterization. Tide dissipation also results from molecular and eddy diffusion. There is a degree of ambiguity between how much of this dissipation comes from the GW momentum force and how much comes from eddy diffusion due to breaking GWs. However, once a GW source spectrum shape to be used in a particular parameterization is chosen, the appropriate magnitude of eddy diffusion can be determined by the tide amplitude profile.

Each of these aspects of the interaction of the tide and gravity waves will be explored in the sections that follow. The focus will be on how the observed tidal structure supplies constraints on the structure of the GW source used in the Alexander and Dunkerton (1999) gravity wave parameterization (ADGWP). In Section 2 we describe the tide model used in this study. Section 3 reviews the formulation of the ADGWP and presents some basic principles relating the GW source spectrum to the

structure of the GW momentum forcing profile. The modulation of the GW force by the tidal winds has a diurnal component that acts as a tidal force that alters the tide structure. We show in Section 4 how the GW forcing of the tide can be understood in terms of the diurnal amplitude of the GW force and the phase shift between the diurnal forcing and the tidal oscillation. The tide model is compared to TIMED and UARS measurements in Section 5. Section 6 shows how the model tide responds to changes in the GW source spectrum. Perhaps the only way to quantify how much GWs contribute to tidal variability is through model experiments. In order to have confidence in the results of such experiments, one must be certain that a GW parameterization is tuned to produce both realistic mean flow and tide structures in the model. This problem is discussed in Section 7. We present our conclusions in a final section.

2. Tide model

Tidal simulations are computed with a time dependent linear primitive equation model. Our model is a linearized version of the spectral non-linear primitive equation model developed by Saravanan (Saravanan and McWilliams 1995). It uses a semi-implicit time-stepping scheme to compute the evolution of the zonal wave 1 component of vorticity, divergence and temperature. All dynamic fields are represented on a horizontal grid in terms of a spherical harmonic expansion truncated at 40 terms for zonal wavenumber 1 only and on 69 pressure levels that are spaced roughly at intervals of 2.5 km from the surface to 170 km.

The tide is forced in the model by heating that varies sinusoidally with local time, and which is confined to a narrow layer in the troposphere prescribed by $AH_{(1,1)}(\phi)V(z)$, with the vertical structure given by $V(z) = \exp(-(z-10)^2/25)$ (where $z = -H\log(p/1000)$ is log-p altitude for p the pressure in mb and H=7 km is the scale height), horizontal structure given by the classical $H_{(1,1)}(\phi)$ Hough mode structure for the migrating tide as a function of latitude ϕ normalized so that $H_{(1,1)}(0) = 1$, and with amplitude $A = 0.8\mathrm{Kd}^{-1}$. This heating rate produces a tide with amplitude equal to the response of the Hough mode component of heating obtained by decomposing the heating

rates derived from the NASA Water Vapor Project (NVAP) data by Lieberman et al., (2003).

The March mean zonal winds from the UARS Reference Atmosphere Project (URAP) (Swinbank and Ortland, 2003) are used for the background winds in the model. Wind values are tapered to zero above the top altitude of the climatology (115 km), and do not effect the tide structure for the altitude range examined in this study. The background temperatures are obtained from the background winds by using the thermal wind relation and the condition that the horizontal average temperature at a given pressure level equals the horizontal average of the climatology derived by Fleming et al., (1990) which has been linearly extrapolated to the model top.

The model tide is damped using both Newtonian cooling and diffusion. The diffusion acts on both the wind and temperature fields. The Newtonian cooling rate profile in K/day, taken from McLandress (2002b), is given by

$$\alpha(z) = 0.05 + 0.3024\exp(-((z - 60)/25)^2) + 0.864\exp(-((z - 105)/15)^2). \quad (1)$$

The diffusive damping used in the model is split between vertical profiles of molecular and eddy diffusion. We use the molecular diffusion values in units of m^2/s taken from Banks and Kocharts (1973):

$$K_{mol}(z) = 3.5 \times 10^{-7} T(z)^{.69} / \rho(z) \quad (2)$$

where $T(z)$ is a global average temperature profile and $\rho(z)$ is the atmospheric density profile in units of kg/m^3. The eddy diffusion is parameterized independently of the GW parameterization and modeled by a profile given by the simple form

$$K_{\text{eddy}} = \frac{K_{\max}}{2}\left(1 + \tanh\left(\frac{z - 80}{10}\right)\right). \quad (3)$$

We will examine the sensitivity of the tide vertical structure to values of $K_{\max}$.

GW force is parameterized using the scheme of Alexander and Dunkerton (1999). It is possible to specify an arbitrary spectrum for the source of GW packets we assume the stress $\rho\overline{u'w'}$ at the source level has a Gaussian spectrum given by:

$$B(c) = B_0 \exp\left(-\left(\frac{c}{c_w}\right)^2\right) \tag{4}$$

where c is the horizontal phase speed for GW propagating in a given azimuth direction, B_0 is the magnitude of the stress at $c = 0$ and c_w gives the $1/e$-width of the spectrum. Each packet is assumed to occur in bins of width $c = 1$ m/s and is present with an intermittency value given by ε. Although it is possible to specify a spectrum that depends on both horizontal phase speed and horizontal wavelength, we specify a representative 'effective' horizontal wavelength of 1000 km.

The waves are launched in four azimuth directions at the Gaussian latitude grid points and at an altitude of 10 km. The source spectra are independent of latitude and azimuth. As will be seen below, the intermittency amounts to a scale factor for the GW force profile. The GW source is also launched at 8 equally spaced points around a latitude circle. The zonal wavenumber 1 component of the global GW forcing is then computed and applied to the momentum equations for the tide.

Figure 1 shows plots of HRDI and TIDI in the top two panels compared to tide model calculations in the bottom panels. The satellite data was collected over a period covering the month of March for two different years for which these instruments were in operation. On any given day the satellite can view at most four different local times on a latitude circle if it views on both sides of the orbit. From day-to-day the local time sample point slowly varies as the orbit precesses. The plots shown here were obtained by binning the meridional wind observations in a local time bin of width one hour centered at 9h. The wind pattern shows the diurnal tide structure quite clearly, but one must keep in mind that the semi-diurnal tide is also present and superimposed on the dominant diurnal tide winds. Both TIDI and HRDI show similar structure in the tide phase, although the TIDI measurements appear to show smaller vertical wavelength and a narrower horizontal structure. This will be discussed further below.

The model simulations shown in Fig. 1 were obtained using the model configuration as already described. The value of $K_{\max} = 50\mathrm{m}^2/\mathrm{s}$ was used for the eddy diffusion profile in both. The second simulation is the same as the first except that the

ADGWP was turned on. The value of the parameter settings and how they were determined is discussed below. The main point here is to note that the vertical wavelength of the model run without GWs, while consistent with other tide models (e.g. Hagan et al., 1995; McLandress, 2002b), is not consistent with observations. Adjustments of damping parameters or mean flow structures cannot fix this discrepancy, and the only mechanism that is able to account for it is the inclusion of GW momentum forcing on the tide.

3. Dynamics of GW forcing

The ADGWP is based on the assumption that GW packets in the source spectrum propagate conservatively until they become convectively unstable. At this point the waves break and deposit all of their momentum to the mean flow at the breaking level. The criterion for wave breaking is the same one derived by Lindzen (1981), where a wave packet with phase speed c, horizontal wavenumber k_{h}, and wave stress $B(c)$ at the source level z_0 breaks at altitude z if $B(c) = B_{break}(c,z)$, for

$$B_{break}(c,z) = \frac{\rho(z)k_{\mathrm{h}}}{2N(z)}(c-u(z))^3, \tag{5}$$

where $\rho(z)$ is the density, $N(z)$ is the buoyancy frequency, and $u(z)$ is the background velocity component in the direction of wave propagation.

The breaking criterion defines $z(c)$, the breaking level of the wave with phase speed c. Generally the breaking level is a discontinuous function of phase speed, since not every altitude will be the breaking level for some GW. We may take the inverse function of the breaking level to define a cutoff phase speed function $c(z)$, which is the phase speed of the wave that breaks at altitude z. The cutoff $c(z)$ defined in this way may be either multivalued or undefined, but we can use it to define a single valued function, also denoted $c(z)$, by setting it equal to the maximum value of all values of $c(z')$ that occur for $z' \le z$. The latter condition reflects the assumption that once a wave breaks it is completely removed from the spectrum at higher levels.

The momentum forcing supplied by the AD scheme may be mathematically expressed as follows. At each level z, the wave stress remaining in the source spectrum resides in the range from $c(z)$ to the maximum phase speed $c_{\max}$ we allow in the spectrum. The acceleration of the background flow due to GW breaking is thus given by:

$$F_{GW}(z) = -\frac{\varepsilon}{\rho(z)}\frac{d}{dz}\int_{c(z)}^{c_{\max}} B(c)dc = \frac{\varepsilon}{\rho(z)}\frac{dc(z)}{dz}B(c(z)). \qquad (6)$$

This formula for the forcing is deceptively simple, but one must keep in mind that the cutoff phase speed depends implicitly on B through (5). However, it does help to understand how the GW forcing profile depends on the shape of the GW source spectrum, as we now try to explain.

The horizontal wavenumber k_h is not another independent parameter in the ADGWP. The saturation criterion does not change for values of k_h and B_0 for which the ratio k_h / B_0 is constant. Therefore, if we multiply the values of k_h and B_0 by a positive factor and divide ε by this factor, the forcing calculated by (6) will remain invariant.

Figure 2 shows examples of the breaking level and the GW forcing profile that occur for GWs propagating through a tidal wind profile. In the top two panels we have chosen GW source spectra that have the same total stress for waves that break above the stratopause, with phase speed extending approximately from $c = 20\ \mathrm{m/s}$ to $c = c_{\max} = 120\ \mathrm{m/s}$, by changing both the width c_w and the amplitude B_0 for the Gaussian shape. All these spectra have roughly the same flux for waves with $c = 50\ \mathrm{m/s}$, with the spectra having larger flux for $c > 50\ \mathrm{m/s}$ and smaller flux for $c < 50\ \mathrm{m/s}$ as c_w is increased. In the bottom two panels we keep the shape of the spectrum constant with $c_w = 60\ \mathrm{m/s}$ while changing the amplitude B_0 and the intermittency ε in a way that keeps the forcing profiles roughly the same magnitude at 70 km.

The left hand panels in Fig. 2 show the wind profile, taken from the meridional wind field of the tide model at latitude 20°S and the breaking levels, with the x-axis giving either wind speed or phase speed for the GWs. The breaking level of a wave at

phase speed c must stay below the critical level where the wind speed $v = c$, but the height of the breaking level may otherwise be adjusted over a considerable range by changing the source flux of the wave. The smaller the flux, the closer the wave will break to the critical level. This principle accounts for the shape of the breaking level curves as we adjust the shape of the source spectra.

The GW forcing profiles, shown in the right panels of Fig. 2, reflect the differences in the breaking level profiles. In the case where c_w is increased, the breaking level for a wave packet with phase speed c is lowered, and the difference between the breaking levels of adjacent waves in the spectrum is decreased. This implies that $dc/dz(z)$ increases at a fixed level as c_w increases. Also, the value of $B(c(z))$ increases with c_w. It follows from (6) that the forcing profile at a given level will increase as we increase c_w. The rate of increase will go up at higher levels because of the density factor, resulting in forcing profiles whose amplitude grows at different rates with altitude. As a general rule, a flatter source spectrum will result in a forcing profile that more strongly increases in amplitude with altitude than a source spectrum that is sharply peaked at low phase speeds. For this reason we find broad source spectra, including sources that follow a power law, to be difficult to work with. After adjusting the intermittency in order to achieve sufficient forcing strength to modify the tide wavelength at 80 km, one will find that the forcing is far too strong at higher levels without imposing further artificial constraints on the GW forcing profile.

For the cases in the bottom panels of Fig. 2 where the amplitude of the source stress is changed while the shape of the source is fixed, the force profile structure shifts in altitude relative to the wind profile. The intermittency was chosen for these cases so that $\varepsilon B(c(z))$ has approximately the same value for values of z ranging from 80-100 km. Thus, the difference in the forcing profiles result from shifts in the profile of $dc/dz(z)$ as the breaking level is lowered by increasing B_0.

So far we have discussed the effects that two independent variations in the 3-dimensional parameter space (B_0, c_w, ε) have on the GW forcing profile. Varying parameters c_w and B_0 in a way that keeps the total source stress constant primarily affects the amplitude growth of the forcing. Varying parameters B_0 and ε in a way that

keeps $\varepsilon B(c(z))$ constant primarily shifts the forcing profile in altitude. A third independent parameter shift in ε alone acts simply as a proportionality factor on the GW forcing profile. We expect these general principles to hold for other GW schemes in use that allow for changes in the GW source spectrum, although details are likely to differ with either the various saturation criteria that are imposed or whether or not it is assumed that waves are totally removed from the propagating spectrum when saturation is reached.

4. Tide modulation of the GW force

We next examine how the GW forcing is modulated by the tide and begin our discussion of how the diurnal component of the GW force will act as a forcing on the tide. The GW tidal forcing is computed by calculating the GW forcing profiles for the background winds over a complete range of local time samples and then taking the diurnal harmonic of the resulting times series. The diurnal component of the tide wind field in an azimuth direction may be expressed as

$$v(t,z) = V(z)\cos(t - \phi_v(z)) \tag{7}$$

where V is the amplitude and ϕ_v is the phase, or local time of maximum amplitude, at altitude z. We may then express the diurnal force as

$$\begin{aligned} F_{GW}(t,z) &= F_c(z)\cos(t - \phi_v(z)) - F_s(z)\sin(t - \phi_v(z)) \\ &= |F|\cos(t - \phi_v(z) + \Delta\phi(z)) \end{aligned} \tag{8}$$

where $|F| = \sqrt{F_c^2 + F_s^2}$ is the GW force amplitude and the phase shift $\Delta\phi$ is the amount that the phase of the GW force leads the phase of the tide.

Ortland (2005a,b) described the effects of forcing on the tide in terms of a complex-valued effective friction coefficient $\gamma = -(F_c + iF_s)/V$. It was shown that a positive friction coefficient ($F_c < 0$, $90^\circ < \Delta\phi < 270^\circ$) decreases tidal amplitude while a negative friction coefficient will enhance tide amplitude. It was also shown that the imaginary part of the friction coefficient will increase the local vertical wavenumber $m(z) = |d\phi_v / dz|$ of the tide when it is negative ($F_s < 0$, $0^\circ < \Delta\phi < 180^\circ$). It is always

the case that $F_s < 0$ for GW forcing computed using the AD scheme. Thus, understanding the phase shift of the GW forcing is important for understanding why some GW schemes will increase tidal amplitude and others will decrease it.

Figure 3 shows the amplitude $|F|$ in the left panels and the phase shift $\Delta\phi$ in the right panels for the GW forcing obtained from the spectra used in Fig. 2. The variation of the spectra when the parameter c_w is varied, as illustrated in the top two panels, primarily affects the shape of the GW forcing amplitude. The forcing for broad spectra is sharply peaked at high altitude while narrow spectra can spread significant GW forcing over a broader altitude range. Typically, power-law source spectra produce forcing profiles similar to the broad Gaussian spectra used here. These spectra all have similar phase shifts relative to the wind profile at altitudes where the forcing amplitude is significant.

The variation of the spectra when the parameter B_0 is varied, shown in the bottom two panels of Fig. 3, primarily affect the relative phase of the GW force. The phase shift is less than 90° for the weak source and we expect the GW forcing to enhance the tide amplitude, since the corresponding effective friction has a negative real part. The strong source, on the other hand, has phase shift greater than 90°, an effective friction that is positive, and will diminish the tide amplitude. The amplitude profile is relatively unaffected below 90 km. The forcing amplitude for the strong GW source drops off rapidly above 95 km because the waves in the spectra with phase speed less than $c_{\max}$ have all become unstable below that altitude. In all of the seven cases shown in Figs. 2 and 3, F_s has a much larger magnitude than F_c and is less than zero. This means that the GW forcing has an effective friction with negative imaginary part and will therefore act to increase the local vertical wavenumber of the tide. The altitude where this increase occurs will depend on the shape and magnitude of the forcing amplitude profile. We will demonstrate the mechanisms discussed here later on in Section 6. Calculations using our tide model will show that the distinct forcing patterns that arise by changing the GW source structure result in distinct patterns in the tide response.

5. Tide model comparisons with data

We have shown in the previous section that variations in the GW parameters result in distinct patterns of variation in the GW diurnal forcing. The fact that the tide

responds differently to each of the GW source parameters makes it possible to apply nonlinear least-squares fitting techniques to determine which parameter settings will provide a fit of the model to observed wind and temperatures. This fitting was performed for the HRDI wind and temperature measurements for March 1993. Along with the three GW parameters, the eddy diffusion parameter $K_{\max}$ and the amplitude of the (1,1) tide mode forced in the troposphere was also adjusted. Adjusting the tide amplitude fits the tide to the observations below 70 km, while the remaining GW and diffusion parameters adjust the model to fit both the tide phase and amplitude. It was found that a submanifold within parameter space gives equally good model fits to the data, and this will be discussed further below. Representative values within this submanifold, which will be used in the examples to follow, are $c_w = 47\mathrm{m/s}$, $B_0 = 0.004\ \mathrm{Pa}$, $\varepsilon = 0.001$ and $K_{\max} = 50\mathrm{m}^2/\mathrm{s}$.

Figure 4 shows the amplitude and phase of the tide in observations of wind and temperature. These observations are compared to model calculations using the GW parameters listed above and to model calculations without GW forcing. The amplitudes and phases in the data were obtained by fitting the diurnal harmonic to data values binned by local time and latitude. The model simulation with GW forcing produces amplitude profiles that follow the measured profiles fairly well. The simulation without GW forcing produces a sharp amplitude peak near 100 km that is not observed in the winds. The amplitude structure in the temperature profile above 100 km cannot be determined from the SABER data, so it is unclear at what altitude the temperature amplitude maximum occurs, but the amplitude growth rate of the model with GW agrees better with the data than for the model without GW. It is possible to tune a model without GW by adjusting the eddy diffusion profile so that the model amplitude profile matches the data (e.g. Khattatov et al. 1997; Yudin et al., 1997), but adjustment of diffusion alone will not bring the model phase into agreement with the measurements. There is a remarkable agreement between the HRDI, TIDI and SABER phase variation with height, and this phase structure is well reproduced in the model simulation with GW forcing but not in the simulation without GW forcing.

The GW force also changes the horizontal structure of the tide. Figure 5 shows the diurnal amplitude in the meridional wind measured by TIDI and the temperature

measured by SABER at 95 km during March 2004. The measurements are compared to model calculations of the amplitude with and without the inclusion of the GW force. We see the addition of GW forcing causes the horizontal structure of the tide to become narrower or more tropically confined. The measurements confirm that the diurnal amplitude in both winds and temperature are narrower than what is obtained in a model without GW forcing. Therefore both the observed vertical and horizontal structures of the migrating diurnal tide indicate that GWs effectively interact with the tide and change its shape.

One explanation for why the GW force narrows the tide horizontal structure was given by Ortland (2005b) in terms of the effective friction coefficient γ. As already discussed in the previous Section, GW forcing may be represented by an effective friction coefficient that has a negative imaginary part. Friction terms γ that do not depend on latitude, when included in the linearized tide equations, modify the frequency σ of the forced modes by $\overline{\sigma} = \sigma + i\gamma$. For GW forcing the modified frequency is decreased in absolute value, since $\sigma < 0$ for the tide and $\mathrm{Im}(\gamma) < 0$. Forced westward Hough modes become equatorially trapped close to the equator as the frequency approaches zero, and both the Lamb's parameter and the vertical wavenumber increase.

6. GW force modulation of tide vertical structure

The calculations of the GW forcing on the tide discussed in Section 4 were done using a fixed tide wind profile. If the GW forcing is strong enough then the tide profile will be altered and the GW forcing structure will naturally change along with it. Thus, once the GW parameterization is switched on in the model, the tide and GW forcing structure will evolve until a stationary state is reached. Before running the tide model to produce the examples shown in this Section, the GW force was computed off line using wind profiles from a model run without GW forcing and the intermittency was adjusted to make the maximum amplitude of the GW force for all cases the same. However when the GW forcing with the spectral parameters so determined is turned on in the model, the GW force and tide mutually adjust until the results shown here are attained. Ultimately the GW force has a different structure than what was engineered using a fixed profile.

Nevertheless, we verify that the tide responds to changes in the GW source spectrum according to the principles described in Section 4. We shall look at examples where the GW source strength is increased or decreased and where the spectral shape is narrowed or broadened relative to the best fit spectrum presented in Section 5. These examples will serve to illustrate the sensitivity of the tide structure to the GW source structure.

Each of Figures 6-10 shows the tide vertical structure represented by the amplitude and phase of the meridional wind profile at 20°S, the latitude-altitude cross section of the diurnal amplitude of the GW force, and the phase of the GW force at 20°S relative to the meridional wind. The top two panels of each figure show the amplitude and phase for the case with no GW force as reference. In these examples the tide has source amplitude that represents the annual average, as prescribed in Section 2.

Figure 6 shows the results for the choice of best-fit source parameters used in Figs. 4 and 5, referred to here as the control experiment. The GW force, with peak amplitude of around 50 m/s/day at 97 km reduces the wind amplitude from 80m/s to 50 m/s, causes the tide phase to decrease more rapidly with height, and has a relative phase greater than 90°. As expected, such a relative phase does cause a decrease in tide amplitude. Significant change in the tide phase is observed above 70 km where the GW force exceeds 5 m/s/day.

Figures 7-8 show the effects of changing the GW source stress by an order of magnitude relative to the control experiment while maintaining the spectral shape. For the experiment shown in Fig. 7 the source stress is decreased, allowing GWs to break at a higher altitude and closer to their critical level. This results in a GW force that is smaller below 80 km, but larger above, and a relative phase that is less than 90°. Because of the decrease in forcing below 80 km, significant change in the tide phase occurs higher than shown in Fig. 6. As expected, the relative phase relationship causes the tide amplitude to increase below 90 km due to GW forcing. However, above 90 km the tide amplitude with GW forcing is smaller than it is without. This is probably due to the diffusive forcing at these levels. The GW forcing increases the local vertical wavenumber of the tide. The diffusive force will therefore also significantly increase because it is approximately proportional to the square of the vertical wavenumber.

The GW source stress is increased for the experiment shown in Fig. 8. Relative to the control run, the GWs break lower, and the upward propagating spectrum is depleted above 105 km. Because of this, the tide amplitude has increased slightly above 105 km because the GW force has been reduced to zero. Also relative to the control run, the maximum GW force amplitude is smaller, but below 80 km the GW force is slightly larger. As a result, we notice significant change in the tide phase at an even lower altitude than in the control run. The relative phase of the GW force has increased, and this is responsible for a decrease in the maximum tide amplitude because there is a stronger component of oscillating GW force that acts out of phase with the tide.

In Figures 9-10 we examine the effect that changing the phase speed width of the GW source spectrum has on the tide. In these examples the GW stress is kept the same at $c = 50\ \mathrm{m/s}$, so that for waves with $c > 50\ \mathrm{m/s}$ that break above 70 km, the narrower spectrum with $c_w = 30\ \mathrm{m/s}$ has smaller source flux and the spectrum with $c_w = 75\ \mathrm{m/s}$ has larger flux relative to the control run. The opposite holds for waves that break below 70 km. These changes in the source spectrum will primarily affect the shape of the vertical forcing profile, as already discussed. In the experiment shown Fig. 9 (with $c_w = 30\ \mathrm{m/s}$), the GW force grows less rapidly with altitude, consistent with what was found earlier. Thus, the GW force strength here is similar to the control case at 80 km and results in a similar tide local vertical wavenumber (i.e. the slope of the phase profile) at this altitude. However, the GW force is stronger below this altitude, so the significant change in the tide phase, as seen in the second panel, starts at 50 km or below.

Some indeterminacy may arise when trying to fit the model to data. If the data quality or range does not extend much below 70 km, there is no way to determine at what altitude the GW force begins to affect the tide. Thus, better constraints on the GW source structure will be obtained when high accuracy wind and temperature measurements are available over a broad region that extends from the stratopause into the lower thermosphere. In Fig. 9 the tide amplitude is severely diminished relative to the control run, even though the maximum GW forcing amplitude is much smaller. Since the amplitude reduction is already considerable near 70 km, the smaller amplitude is probably due to the stronger GW force in the lower mesosphere.

In the final example shown in Fig. 10 (with $c_w = 75\ \mathrm{m/s}$) the GW force has a sharp peak at 95 km. This is typical for 'flat' source spectra and quite similar to the forcing profiles we obtain when using a power-law spectra for the GW source. Little significant amplitude or phase change occurs in the tide below 85 km. It is possible to lower the forcing profile by also adjusting the source stress factor B_0. Once again, it should be possible to determine whether or not the GW force profile is sharply increasing if the altitude range of the observations is sufficiently large.

7. Discussion

Modelers typically tune a GW parameterization so that the model zonal mean flow resembles observed climatology. We have taken a different approach by tuning the ADGWP so that our tide model reproduces the observed tidal structures. The question remains whether or not the GW parameter settings we have found here will also reproduce zonal mean flow climatology if used in a 2-dimensional model. This issue is beyond the scope of the present paper, but in this section we will examine the related question of how the GW parameterization settings used by Garcia and Solomon (1985) affect the tide in our model.

Garcia and Solomon (hereafter GS) used the Lindzen parameterization with phase speeds c from -40 to 40 m/s at 10 m/s intervals. The horizontal wavelength is 100 km, the intermittency is $\varepsilon = .12$ and the source momentum flux is given by

$$\left|\overline{u'w'}\right| = 10^{-2} \exp(-(c/30)^2) \sin|2\theta| \ \ \mathrm{m^2 s^{-2}} \tag{9}$$

at the source level of 16 km, where θ is latitude. For density $\rho(16) = .13\ \mathrm{kg\ m^{-3}}$ at the source, this translates to a stress spectrum with, $B_0 = 1.3 \times 10^{-3}\ \mathrm{Pa}$. As explained in Section 3, equivalent results are obtained using a source stress with B_0 a factor of 10 smaller if the horizontal wavelength is 1000 km.

The ADGWP becomes the Lindzen parameterization with a simple modification. Instead of setting the GW flux equal to zero after a wave breaks, we set the flux equal to the minimum of the saturation flux, given by the right hand side of (5), and the flux at the previous level. This modification was made in our model and the effects of the GS

parameter values on the tide were calculated. Figure 11 shows the results of this run, compared to both the control run (Fig. 6) and the run with no GW force. There are several features of this experiment which we shall describe.

First, note that the amplitude of the tide between 75 and 90 km has increased relative to the simulation with no GW force. Also note that the structure of the tide amplitude profile is similar to the amplitude profile in Fig. 7, which was obtained using the same value of $c_w = 30 \text{ m/s}$. The amplitude profile is qualitatively similar to the control run, except between 85-95 km. As noted before, the tide amplitude increase happens when wave flux is deposited with phase relative to the tide less than 90°. With the Lindzen scheme, waves continue to propagate upward beyond the breaking level, causing an upward shift of the total flux profile relative to what is calculated using the ADGWP. Starting with the same source spectrum, the forcing profile calculated using the Lindzen scheme will therefore be somewhat larger, due to the density effect, and shifted upward relative to the ADGWP. The upward shift in the forcing profile results in a relative phase between the GW force and the tide that typically 20° less than with ADGWP. In this example, the relative phase is considerably less than 90° throughout the mesosphere (not shown) and therefore the GW forcing causes a tide amplitude increase.

Second, the amplitude of the GW force is twice as strong as in previous examples, and yet the phase structure of the tide response is close to that of the control run. In order to accomplish this, there are at least three main differences, besides the GW source spectrum, between this experiment and the control run. One difference is that the forcing used in the experiment shown in Fig. 11 is only applied in the zonal direction. We have found that GW forcing calculated with any GW scheme applied in the meridional direction acts twice as effectively on the tide as in the zonal direction. That is, the amplitude of the GW force in the zonal direction must be twice as large as the forcing in the meridional direction in order to accomplish the same tide phase shift or the same tide amplitude modification. Thus, if we were to assume that the GW source is isotropic in azimuth, we would find that the GW forcing with the GS parameters would produce a tide with unrealistic phase structure. Even with just the GW force applied in the zonal direction, the GS parameters produce an unrealistic tide horizontal structure, as illustrated in the lower right panel of Fig. 11.

Two other differences between the GS experiment and the control run are the low maximum phase speed at 40 m/s and the latitudinal variation of the total GW source flux. The ADGWP will produce no GW force above the altitude where the wave with the maximum phase speed breaks, so such a low maximum phase speed is not a viable option with this scheme. The Lindzen scheme allows waves to propagate at a saturated level once they break, so GW forcing is produced until a critical level is encountered at the maximum phase speed. If we extend the maximum phase speed in the Lindzen scheme to 100 m/s, in line with what is useable with the ADGWP, we find that the GW forcing is again too strong and produces unrealistic phase structure in the model tide. It is not satisfactory to have acceptable model results to depend on an artificially chosen parameter, such as the maximum phase speed, unless there is some physical reason to expect that the GW spectrum does indeed cut off at 40 m/s.

The latitudinal variation in total GW source flux causes the peak diurnal force to occur at mid-latitudes, as shown in the bottom left panel of Fig. 11. If the GW source is assumed to be uniform in latitude with the maximum total flux value used here, then the GW force will be strongest in the subtropics. Since the tide winds maximize in the subtropics, the GW force will have a larger effect on the tide than it did here and again an unrealistic tide phase structure will occur. This example serves to illustrate the difficulty with satisfying the requirements for finding GW source parameters that give a GW force that is strong enough to produce a realistic mean flow with jet reversals during solstice in the thermosphere, and yet weak enough to not affect the tide too strongly in a way that produces unrealistic phase or amplitude structures. Perhaps a solution to balancing both requirements involves exploring other latitude distributions for the total GW flux, latitudinal variations in the intermittency, and GW sources that are anisotropic in azimuth, as well as searching for other candidates for the GW source spectrum.

Finally, we note that the amplitude increase in the tide would have been much larger if we had not also used a larger value $K_{\max} = 100\ \mathrm{m^2 s^{-1}}$ for the eddy diffusion than was used in the control run. Since the amplitude of the tide can be controlled by both the eddy diffusion and the GW force, this serves to illustrate a degree of ambiguity in how much the tide structure constrains the GW parameter settings. This ambiguity gives rise to a null space, a submanifold in parameter space that represents all of the GW

parameters that produce the same effect on the tide. As was discussed in the previous section, decreasing the total flux in the GW source spectrum decreases the relative phase between GW force and tide and therefore decreases the amount of damping due to the GW force. The decrease in damping can be offset by simultaneously increasing the eddy diffusion. This tradeoff in GW parameters illustrates a 1-parameter subset of the null space.

Resolving this ambiguity in parameter space requires further constraints that must be provided by either observations of GW fluxes or by examining the properties that GW forcing has on other aspects of model dynamics. There also appears to be a fundamental difference between the way that the Lindzen parameterization and ADGWP act on the tide, since for a given source spectrum, the relative phase between tide and GW force will come out quite differently between the two. It may be possible to find different source spectra to use in each parameterization that enables each scheme to have the same effect on the tide, but one must then also make sure that the zonal mean forces that are produced in each are the same as well. One must also try to avoid the undesirable situation, which occurred in the example here, where a physical model parameter such as eddy diffusion is tuned to produce realistic results, and yet depends on the GW parameterization scheme that is used in the model.

8. Conclusions

We have shown that the observed tide vertical and horizontal structures can be reproduced in a tide model that includes GW interaction with the tide. The phase structure of the tide is directly related to the amplitude of the diurnal component of the GW force, and the observed phase therefore provides a constraint on this amplitude profile. Where the tide phase begins to differ from the classical phase structure indicates the altitude where the GW force becomes significant, which is in turn related to the shape of the GW source spectrum. One estimate for the magnitude and structure of the GW force that produces realistic tide structure in our model is provided by the experiment shown in Fig. 6. This estimate was obtained using the ADGWP under the assumption that the GW source spectrum was uniform in latitude and isotropic in azimuth. If the GW source is isotropic in azimuth, we find that the GW force in the meridional direction is much more effective than GW force in the zonal direction in changing tide structure.

Therefore, under the isotropy assumption, the results of this paper may be viewed as providing constraints on the meridional GW forcing. However, a GW scheme that is tuned to produce a realistic mean flow may also produce zonal diurnal forcing that too strongly affects the tide. In this case, our results may be used as a guide to find alternate GW parameters and their latitude and azimuth dependence that will allow the model to produce realistic mean flow and tide structures.

We have also described basic principles that govern how the diurnal component of GW momentum forcing, modulated by tidal winds, depends on the shape of the GW source spectrum and how the diurnal component of the GW force acts on the tide and changes its structure. They may be summarized as follows. Increasing the amplitude of the diurnal component of GW force will increase the rate that the tide phase changes with altitude. The GW force will become more in phase with the tide if the GW source strength is weakened, because waves will then break higher. When the relative phase of the GW force becomes less than 90°, the tide amplitude will increase as a result of GW forcing. These principles will apply to all GW parameterization schemes currently in use. However, various schemes may have different effects on the tide even if they employ the same source spectrum because the altitude where the bulk of the GW momentum is deposited will determine the relative phase between the GW forcing and the tide. This may constitute a fundamental difference between GW schemes if the schemes cannot be tuned to produce the same forcing on both the mean flow and tide.

Understanding the interaction of the tide and gravity waves is important for understanding the mechanism behind the seasonal variability of the tide. The observed seasonal variation in tide amplitude has maxima during equinox and minima near solstice. The equinox maxima change significantly from year-to-year (Vincent et al., 1998). The tide amplitude variability cannot be explained by variability in the tropospheric water vapor heating, which is the primary source of the migrating diurnal tide. Other potential sources for tide variability are latent heat release (Hagan and Forbes, 2002), interaction with the zonal mean winds (McLandress, 2002b), GW interaction with the tide (Mayr et al., 1998; Meyer, 1999) and seasonally varying eddy diffusion (Khattatov et al., 1997; Hagan et al., 1999). Each of these mechanisms can be shown to produce tide variability in a model. If we are to have confidence in any

conclusions regarding the role that gravity waves play in tide variability, it must be shown that the gravity wave scheme used in the model not only reproduces realistic zonal mean winds and temperatures and realistic tide amplitude but also realistic tide phase structure.

Acknowledgements

This work was supported by NASA contracts NASW-00016, NASA C78C, and NAG5-5334. We thank Han-Li Liu and an anonymous reviewer for their valuable comments.

References

Akmaev, R. A. (2001), Simulation of large-scale dynamics in the mesosphere and lower thermosphere with the Doppler-spread parameterization of gravity waves 2. Eddy mixing and the diurnal tide, *J. Geophys. Res.* **106**, 1205-1213.

Akmaev, R. A., V. A. Yudin and D. A. Ortland (1997), SMLTM simulations of the diurnal tide: comparison with uars observations. *Ann. Geophysicae* **15,** 1187-1197.

Alexander, M. J., and T. J. Dunkerton (1999), A spectral parameterization of mean-flow forcing due to breaking gravity waves, *J. Atmos. Sci.*, **56**, 4167-4182.

Banks, P. M., and G. Kockarts, (1973) Aeronomy, part B, 355 pp., Academic, San Diego, Calif.

Fleming , E., L., S. Chandra, J. J. Barnett and M. Corney, (1990). Zonal mean temperature, pressure, zonal wind and geopotential height as functions of latitude, *Adv. Space Res.,* **10**, 1211-1259.

Fritts, D. C., and R. A. Vincent (1987), Mesospheric momentum flux studies at Adelaide, Australia: Observations and a gravity wave-tidal interactions model. *J. Atmos. Sci.* **44**, 605-619.

Garcia, R. R., and S. Solomon (1985), The effect of breaking gravity waves on the dynamics and chemical composition of the mesosphere and lower thermosphere, *J. Geophys. Res.* **90,** 3850-3868.

Hagan, M. E., M. D. Burrage, J. M. Forbes, J. Hackney, W. J. Randel, X. Zhang (1999), GSWM-98: Results for migrating solar tides. *J. Geophys. Res.* **104**, 6813-6827.

Hagan, M. E., and J. M. Forbes (2002), Migrating and nonmigrating diurnal tides in the middle and upper atmosphere excited by tropospheric latent heat release, *J. Geophys. Res.*, **107**(D24), 4754, doi:10.1029/2001JD001236 .

Hagan, M. E., J. M. Forbes, and F. Vial (1995), On modeling migrating solar tides. *Geophys. Res. Let.* **22**, 893-896.

Isler, J. R., and D. C. Fritts (1996), Gravity wave variability and interaction with lower-frequency motions in the mesosphere and lower thermosphere over Hawaii. *J. Atmos. Sci,* **53**, 37-48.

Khattatov, B. V., M. A. Geller, V. A. Yudin, and P. B. Hays (1997), Diurnal migrating tide as seen by the high-resolution Doppler interferometer/UARS, 2, Monthly mean global zonal and vertical velocities, pressure, temperature and inferred dissipation. *J. Geophys. Res*. **102** 4423-35.

Lieberman R. S., D. A. Ortland, and E. S. Yarosh (2003), Climatology and interannual variability of diurnal water vapor heating, *J. Geophys. Res., 108* (D3), 4123, doi:10.1029/2002JD002308.

Lindzen, R. S. (1981) Turbulence and stress owing to gravity wave and tidal breakdown, *J. Geophys. Res.* **86** 9707-14.

Liu, H.-L., and M. E. Hagan (1998), Local heating/cooling of the mesosphere due to gravity wave and tidal coupling. *Geophys. Res. Lett.* **25**, 2941-2944.

Mayr, H. G., J. G. Mengel, K. L. Chan and H. S. Porter (1998) Seasonal variations of the diurnal tide induced by gravity wave filtering. *Geophys Res. Lett.* **25**, 943-946.

McLandress, C. (1998), On the importance of gravity waves in the middle atmosphere and their parameterization in general circulation models. *J. Atmos. Solar-Terr. Phys*. **60**, 1357-1383.

McLandress, C. (2002a), The seasonal variation of the propagating diurnal tide in the mesosphere and lower thermosphere. Part I: The role of gravity waves and planetary waves, *J. Atmos. Sci.,* **59,** 893-906.

McLandress, C. (2002b), The seasonal variation of the propagating diurnal tide in the mesosphere and lower thermosphere. Part II: The role of tidal heating and zonal mean winds. *J. Atmos. Sci.,* **59,** 907-922.

Meyer, C. K. (1999), Gravity wave interactions with the diurnal propagating tide. *J. Geophys. Res.,* **104,** 4223-4239.

Ortland, D. A., (2005a), Generalized Hough Modes: The Structure of Damped Global-Scale Waves Propagating on a Mean Flow with Horizontal and Vertical Shear. *J. Atmos. Sci.,* **62,** 2674–2683.

Ortland, D. A. (2005b), A Study of the Global Structure of the Migrating Diurnal Tide Using Generalized Hough Modes. *J. Atmos. Sci.*, **62**, 2684-2702.

Saravanan, R., and J. C. Mc Williams (1995), Multiple equilibria, natural variability, and climate transitions in an idealized ocean–atmosphere model**.** *Journal of Climate*: **8,** 2296–2323.

Swinbank, R., and D. A. Ortland (2003), Compilation of wind data for the Upper Atmosphere Research Satellite (UARS) Reference Atmosphere Project, *J. Geophys. Res.*, *108*(D19), 4615, doi:10.1029/2002JD003135.

Vincent, R. A., S. Kovalam, D. C. Fritts, J. R. Isler (1998) Long-term MF radar observations of solar tides in the low-latitude mesosphere: Interannual variability and comparisons with the GSWM. *J. Geophys. Res.* 103(D8): 8667-8883.

Wang, D. Y. and D. C. Fritts (1991), Evidence of gravity wave-tidal interaction observed near the summer mesopause at Poker Flatt, Alaska. *J. Atmos. Sci.* **48,** 572-583.

Yudin, V. A., B. V. Khattatov, M. A. Geller, D. A. Ortland, C. McLandress, and G. G. Shepherd (1997), Thermal tides and studies to tune a mechanistic tidal model using UARS observations. *Ann. Geophys.* **15** 1205-1220.

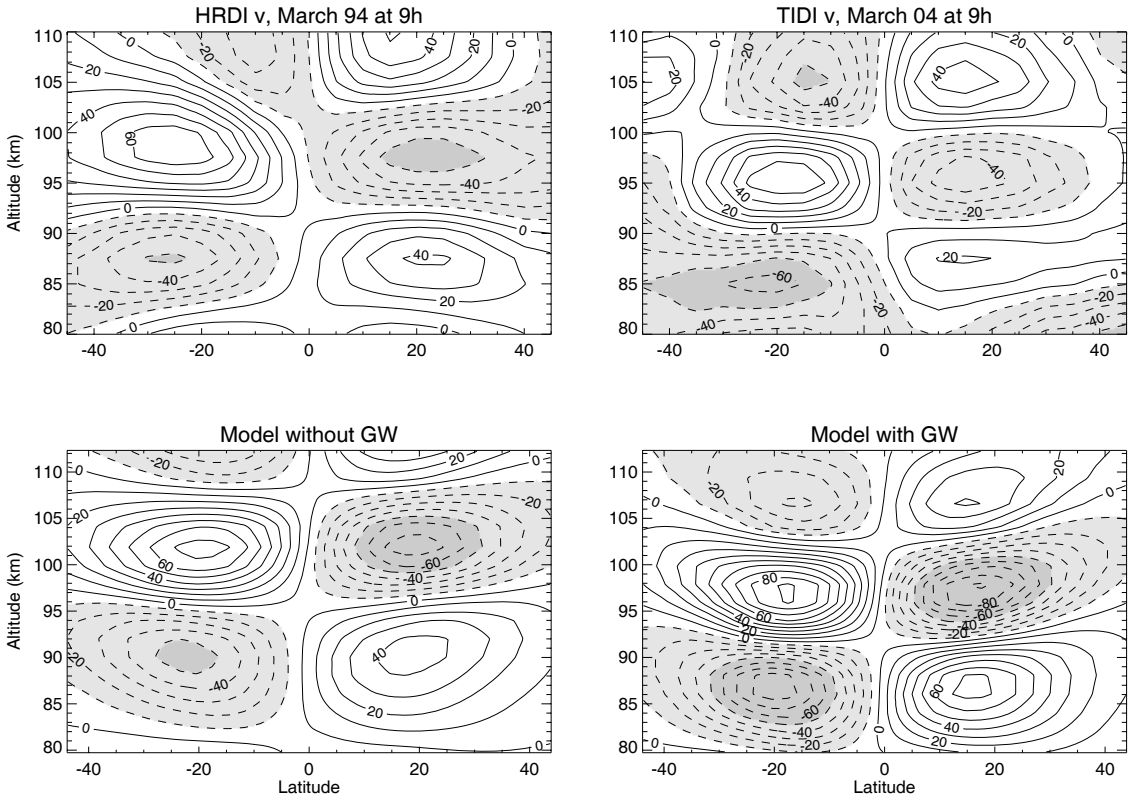

Figure 1. Meridional winds measured in March at local time 9 hours from HRDI (top left) during 1993 and TIDI (top right) during 2004. These are compared to model simulations without (bottom left) and with (bottom right) the effects of GW momentum forcing of the tide. The contour interval is 10 m/s, with negative values shaded.

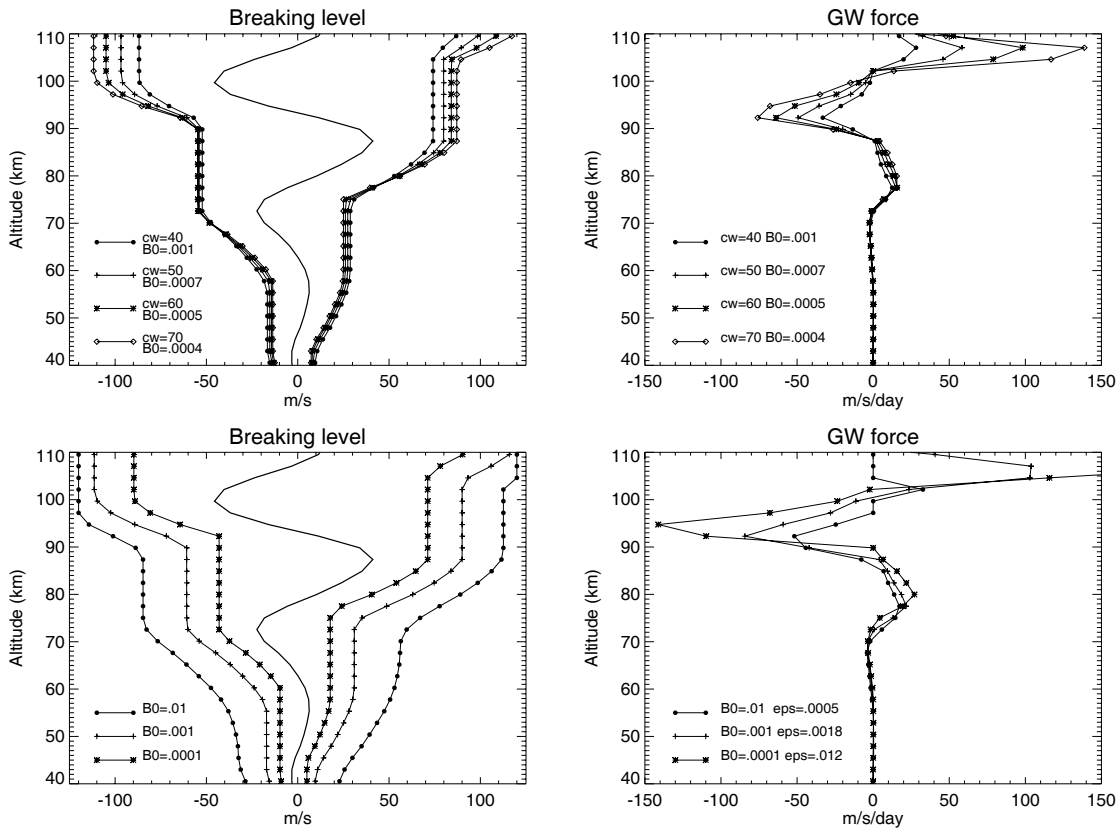

Figure 2. The left panels show a tidal wind profile and the breaking levels (curves with symbols) for gravity waves for a variety of source spectra. The x-axis labels the wind or phase speed. The right panels show the GW momentum force corresponding to each example. $c_w = 60$ m/s for the examples in the bottom panels.

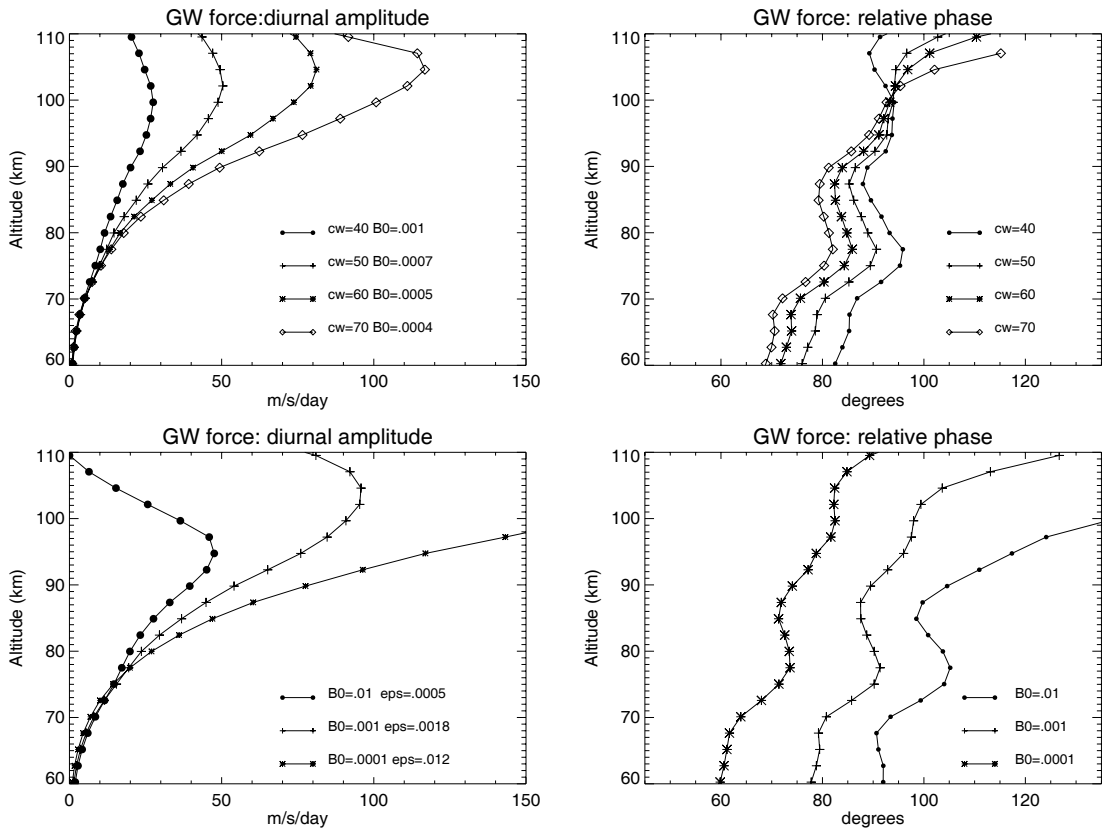

Figure 3. The left panels show the diurnal amplitude of the GW force calculated for tide meridional winds using various source spectra in the ADGWP. The right panels show the phase difference between the diurnal component of the GW force and the tide winds in each of the examples. $c_w = 60$ m/s for the examples in the bottom panels.

i

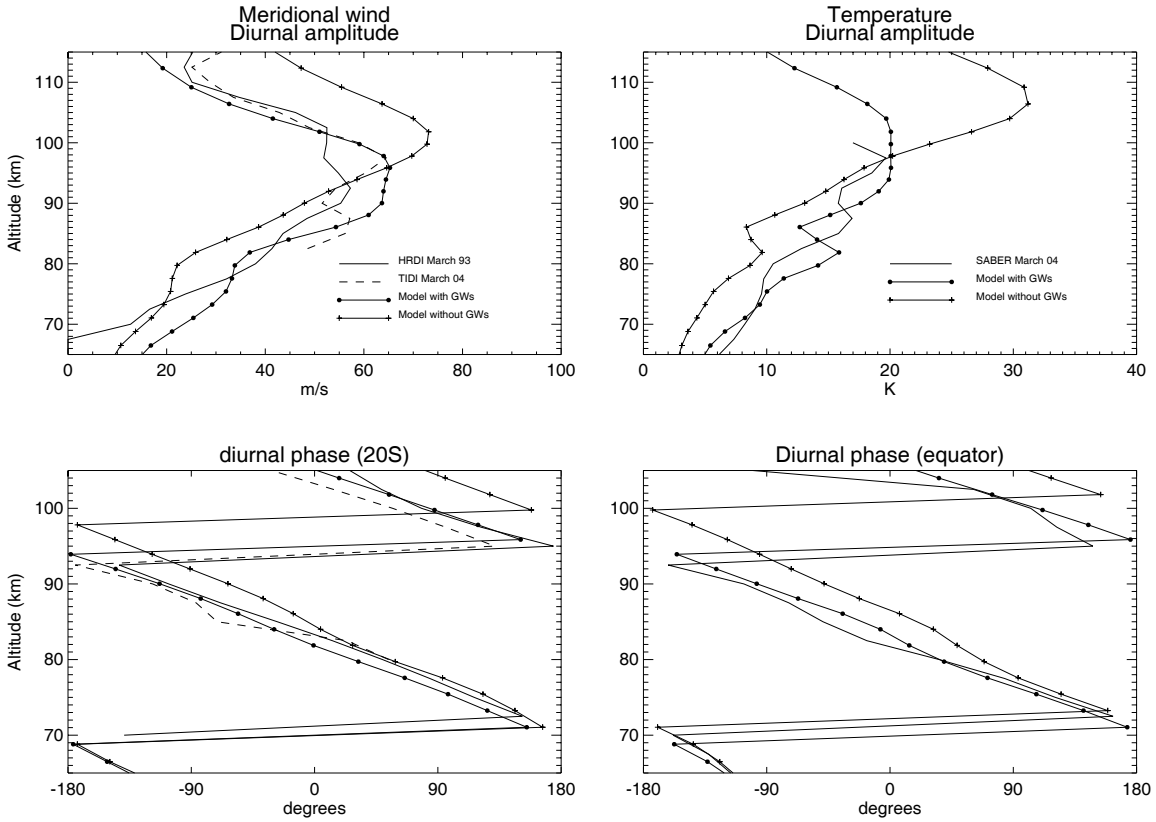

Figure 4. Left: Diurnal amplitude (top) and phase (bottom) of the HRDI, TIDI and model meridional winds shown in Fig. 1 at latitude 20°S. Right: Diurnal amplitude (top) and phase (bottom) of the SABER and model temperatures at the equator.

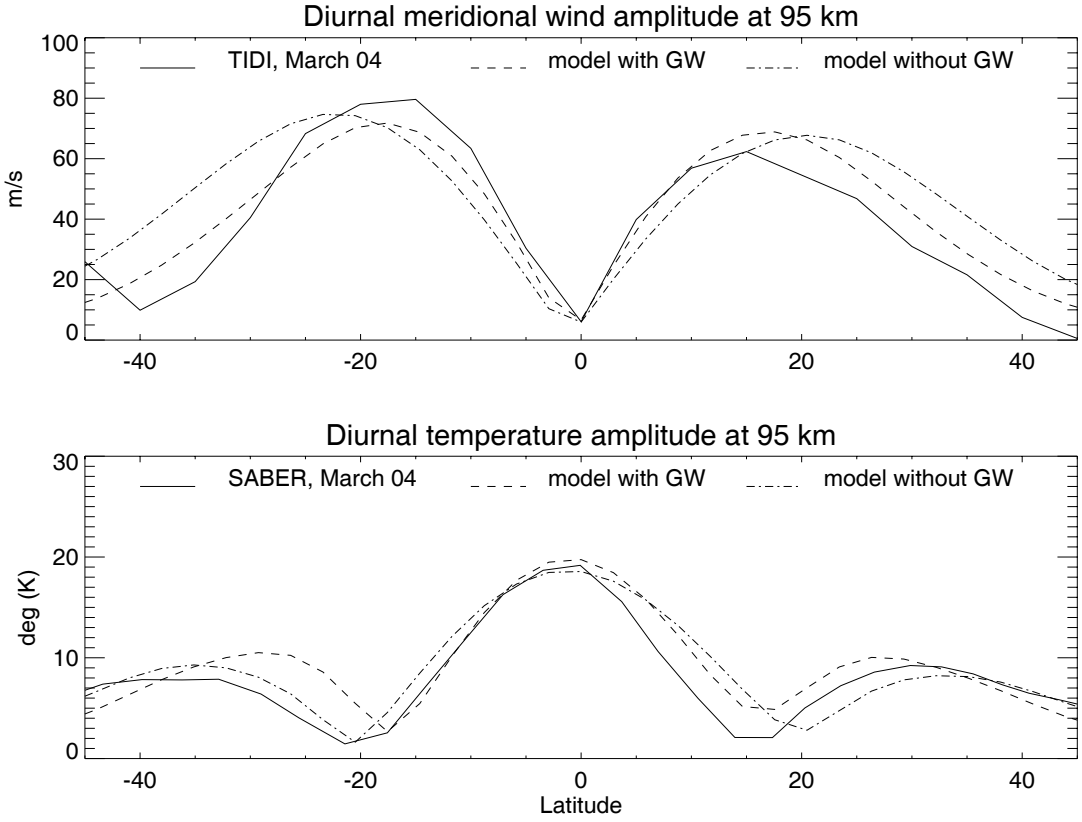

Figure 5. Diurnal amplitude of the meridional winds measured by TIDI (top) and of the temperature measured by SABER (bottom) at 95 km during March 2004. The measurements are compared to two model simulations with and without GW forcing of the tide.

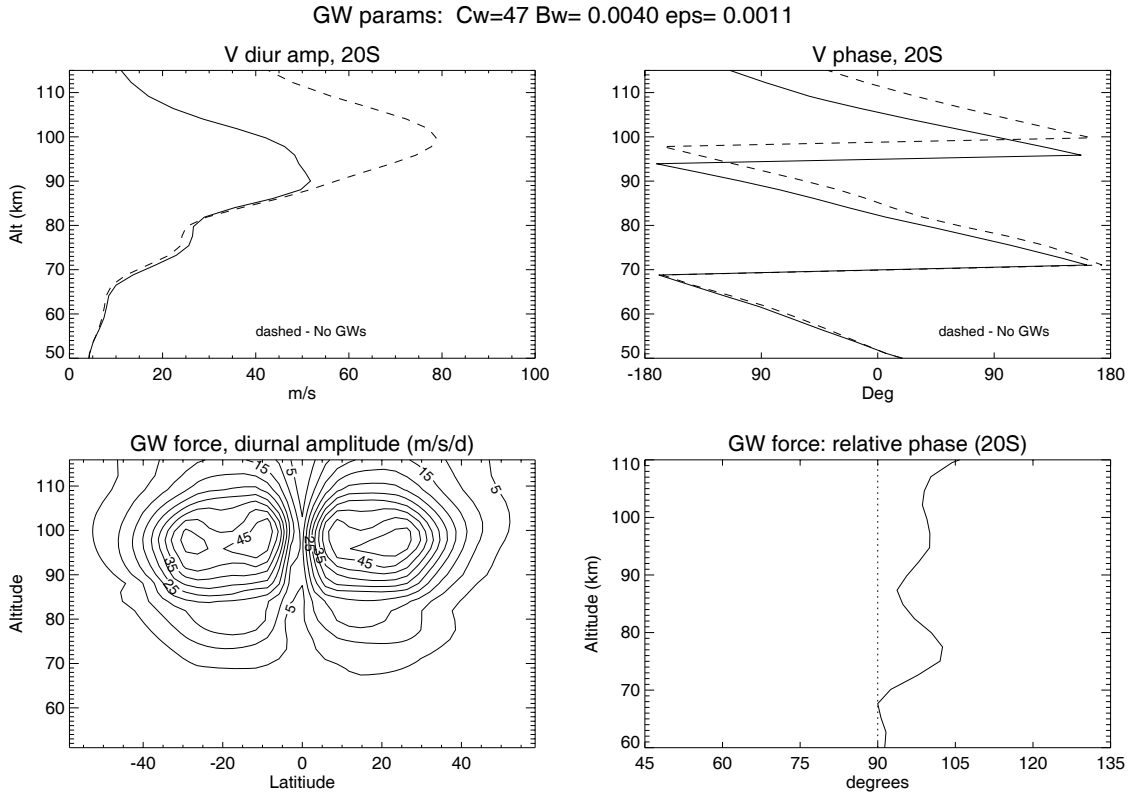

Figure 6. Model simulation of the tide coupled with GW forcing using a source spectrum with phase speed width $c_w = 47\mathrm{m/s}$, stress $B_0 = 0.004$ Pa, and intermittency $\varepsilon = 0.0011$. Top left: Meridional wind diurnal amplitude at 20°S with GW force (solid), and without GW force (dashed). Top right: Phase of the meridional wind with (solid) and without (dashed) GW force. Bottom left: Diurnal amplitude of the GW force (contour interval is 5 m/s/day). Bottom right: phase difference between the diurnal component of the GW force and the meridional wind at 20°S.

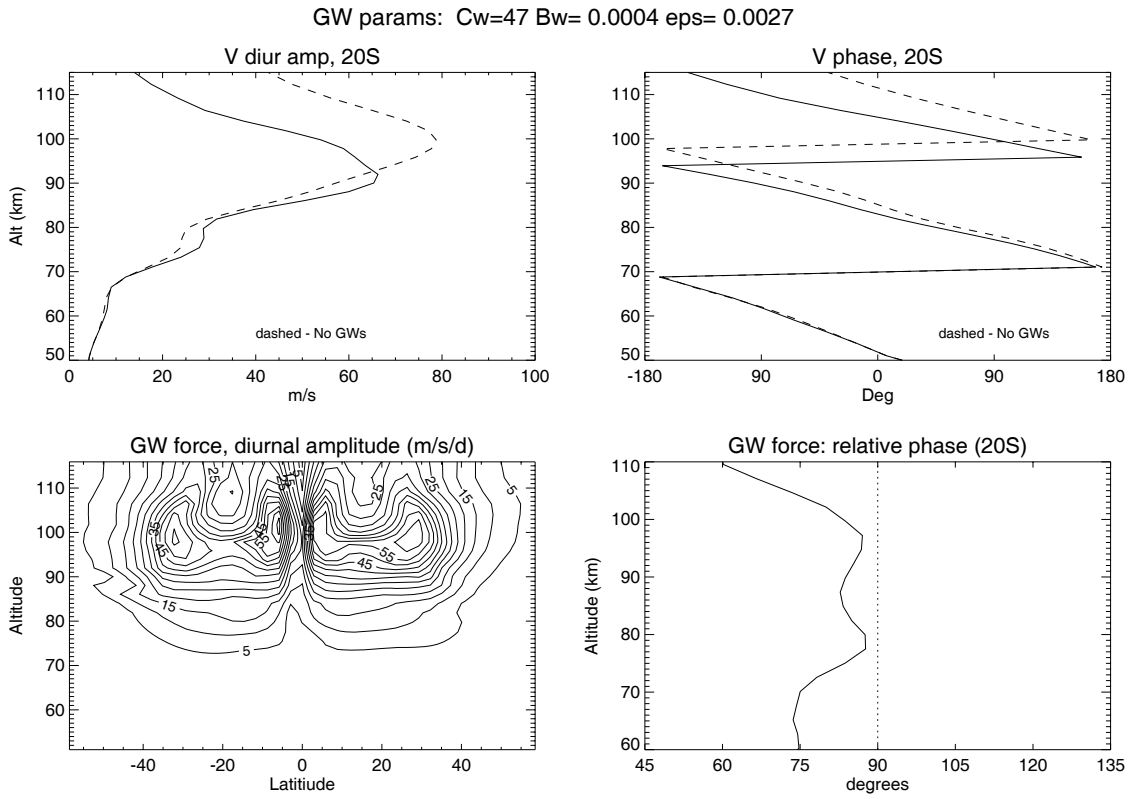

Figure 7. Same as Fig. 6, for $c_w = 47\mathrm{m/s}$, $B_0 = 0.0004$ Pa, and $\varepsilon = 0.0027$.

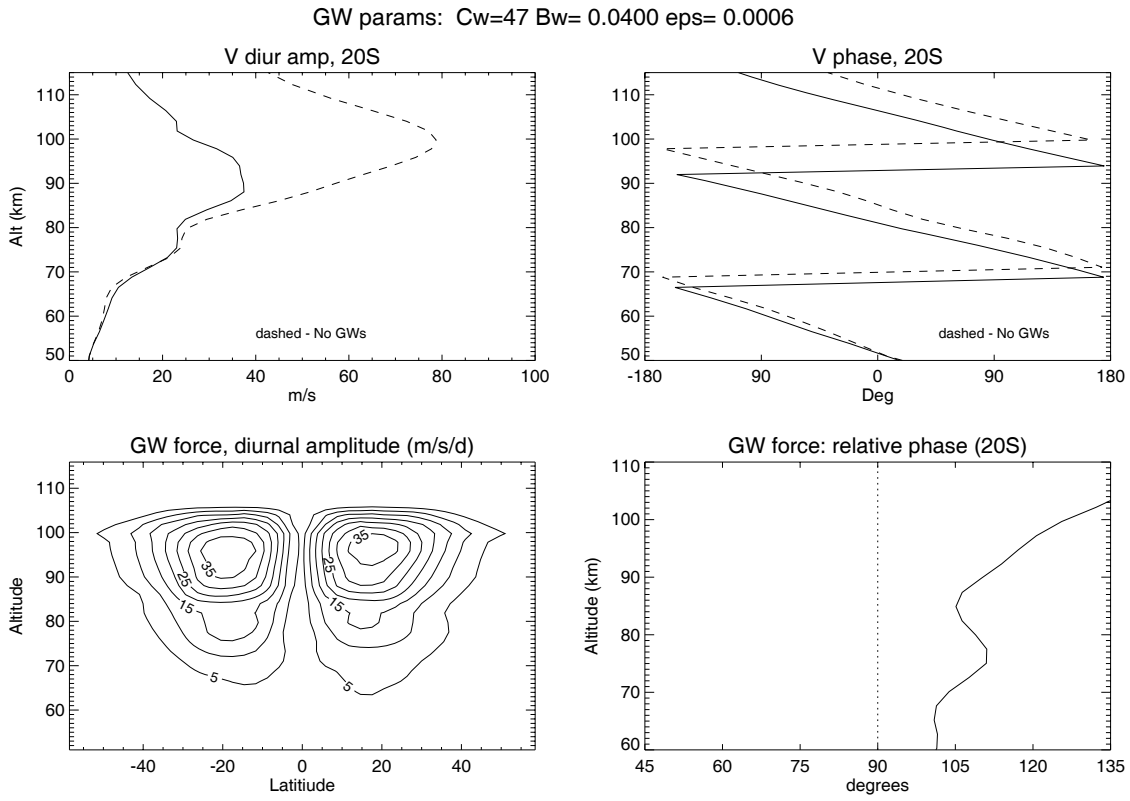

Figure 8. Same as Fig. 6, for $c_w = 47\mathrm{m/s}$, $B_0 = 0.04$ Pa , and $\varepsilon = 0.0008$.

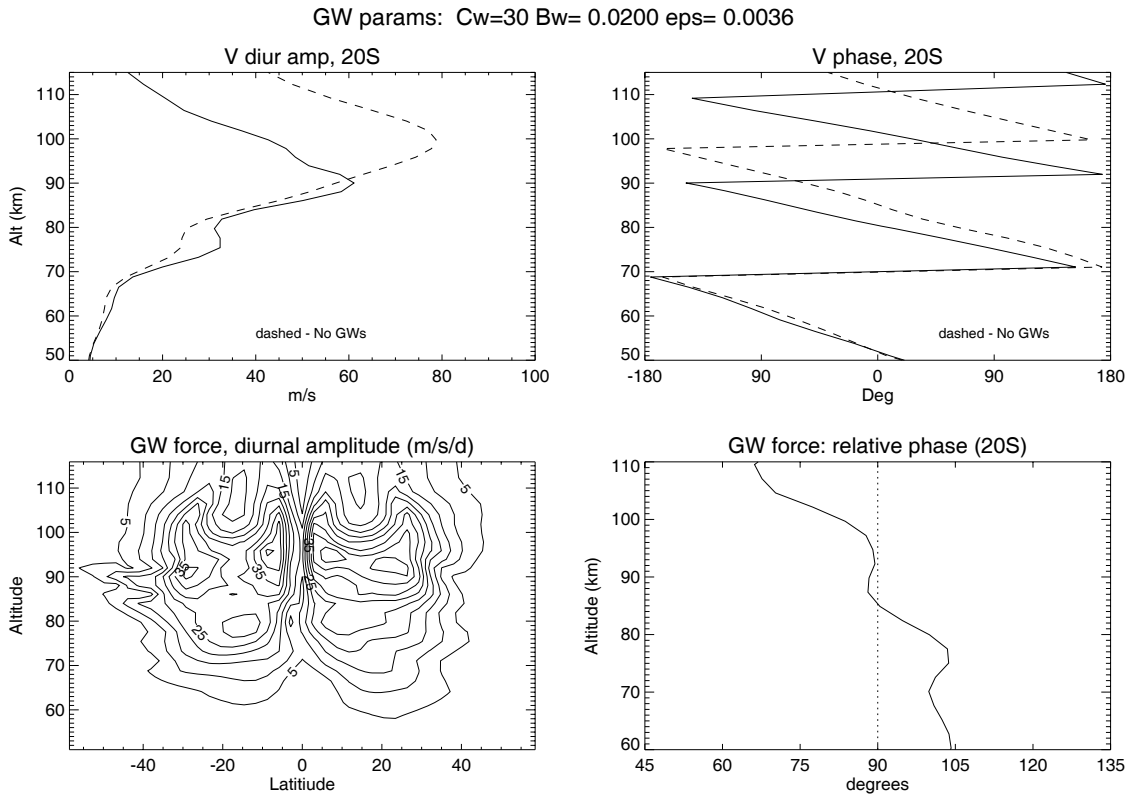

Figure 9. Same as Fig. 6, for $c_w = 30\mathrm{m/s}$, $B_0 = 0.02$ Pa , and $\varepsilon = 0.0038$.

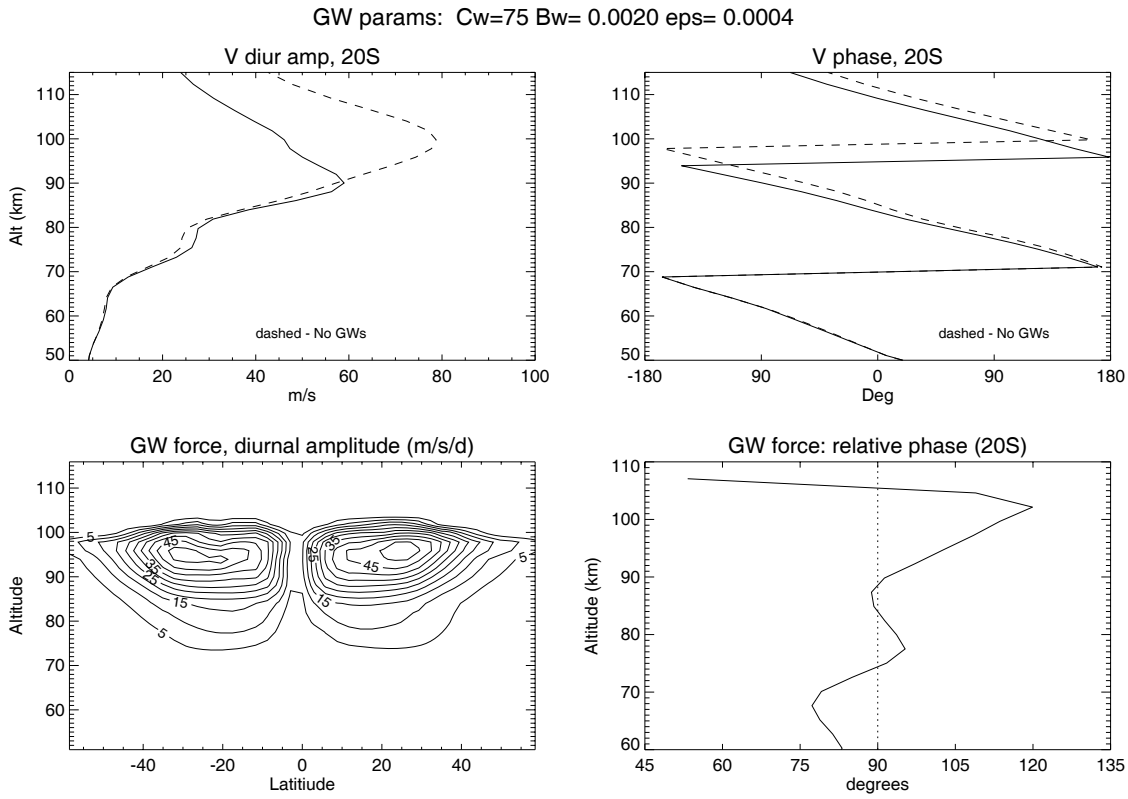

Figure 10. Same as Fig. 6, for $c_w = 75\mathrm{m/s}$, $B_0 = 0.002$ Pa , and $\varepsilon = 0.0004$.

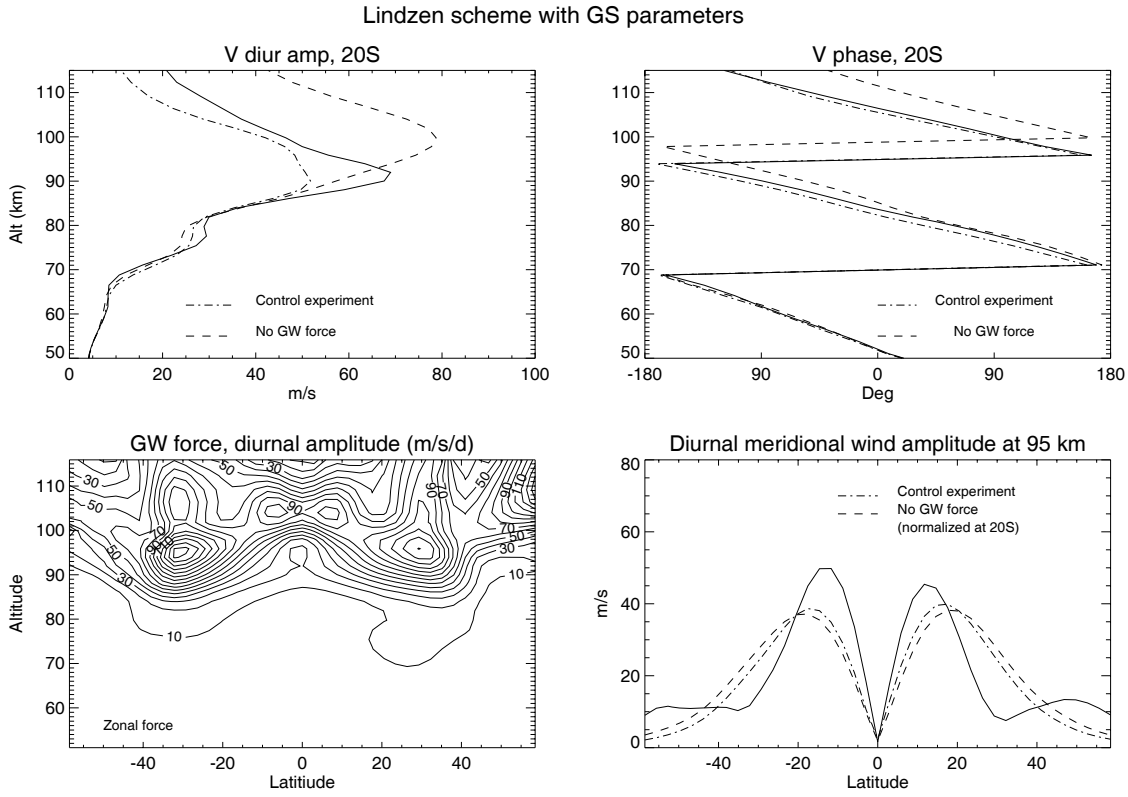

Figure 11. Model simulation of the tide coupled with GW forcing calculated using the Lindzen GW scheme using a source spectrum with parameters from Garcia and Solomon (1985). Top left: Meridional wind diurnal amplitude at 20°S with GW force compared to a simulation without GW force and to the control run from Fig. 6. Top right: Phase of the meridional wind at 20°S. Bottom left: Diurnal amplitude of the GW force in the zonal direction (contour interval is 10 m/s/day). Bottom right: Diurnal amplitude of the meridional wind at 95 km.